

A Locked Nucleic Acid-Based Nanocrawler: Designed and Reversible Movement Detected by Multicolor Fluorescence

I. Kira Astakhova,* Karol Pasternak, Meghan A. Campbell, Pankaj Gupta, and Jesper Wengel*

Nucleic Acid Center and Biomolecular Nanoscale Engineering Center, Department of Physics, Chemistry and Pharmacy, University of Southern Denmark, Campusvej 55, 5230 Odense M, Denmark

S Supporting Information

ABSTRACT: Herein we introduce a novel fluorescent LNA/DNA machine, a nanocrawler, which reversibly moves along a directionally polar complementary road controlled by affinity-enhancing locked nucleic acid (LNA) monomers and additional regulatory strands. Polyaromatic hydrocarbon (PAH) dyes attached to 2'-amino-LNA monomers are incorporated at four stations of the system, enabling simple detection of the position of the nanocrawler via a step-specific color signal. The sensing is provided by highly sensitive, chemically stable, and photostable PAH LNA interstrand communication systems, including pyrene excimer formation and pyrene–perylene interstrand Förster resonance energy transfer. We furthermore demonstrate that the nanocrawler selectively and reversibly moves along the road, followed by a bright and consistent fluorescence response for up to 10 cycles without any loss of signal.

Monitoring the movement of biomolecular nanodevices by a simple and effective method under native conditions is an important goal within nucleic acid nanotechnology. Efficient, rapid, and simple monitoring could further stimulate the design, preparation, and applications of diverse DNA nanomachines within, for example, molecular diagnostics¹ and imaging.² Fluorescence is a convenient sensing method for these applications, which require the use of fluorophores that are photostable and chemically stable and simultaneously provide high fluorescence quantum yields. The fluorescence of such molecules can be rapidly detected by a simple change of color without the need for additional procedures or equipment.^{1a} The Cy3–Cy5 Förster resonance energy transfer (FRET) pair has already been applied in imaging of large DNA nanostructures.^{1,3} Furthermore, efficient hybridization following the Watson–Crick base-pairing rules is required for the efficient assembly of the diverse building of a nucleic acid nanodevice. 2'-Amino-substituted locked nucleic acid (LNA) monomers having polyaromatic hydrocarbon (PAH) dyes attached to the 2'-amino group meet these requirements and are therefore very promising as constituents of nucleic acid nanodevices.^{4,5}

Cyclic oligonucleotides are appealing structural elements for DNA nanotechnology⁶ and can be prepared by either chemical⁷ or enzymatic⁸ ligation reactions. Enzymatic cyclization of synthetic 40–200 nucleotide (nt) oligonucleotides using T4 DNA ligase, developed by Diegelman and Kool,⁸ is an effective method that gives the desired cyclic DNA in sufficient yields.

Enzymatic ligation requires the incorporation of a 5'-terminal phosphate group on the oligonucleotides and intramolecular annealing to a 15–20 nt splint sequence to bring the terminal groups into close proximity. Enzymatic ligation has already been used for the preparation of various cyclic oligonucleotides,⁸ although the chemically modified analogues (currently gaining increased attention in research and clinical studies)⁹ to the best of our knowledge have not been cyclized in this way.

Herein we report a novel cyclic DNA machine, an LNA/DNA nanocrawler, which was prepared by enzymatic ligation and moves reversibly along its complementary road with high selectivity, as monitored by specific fluorescence signals at designed stations along the road. This strategy provides a novel platform for an easily detectable and dynamic multistep system.

Our design is shown in Figure 1. The complementary pair ^cNC1:R1 (fluorescent nanocrawler:road) includes four stations with specific interstrand communication units M^1 – M^3 at each of

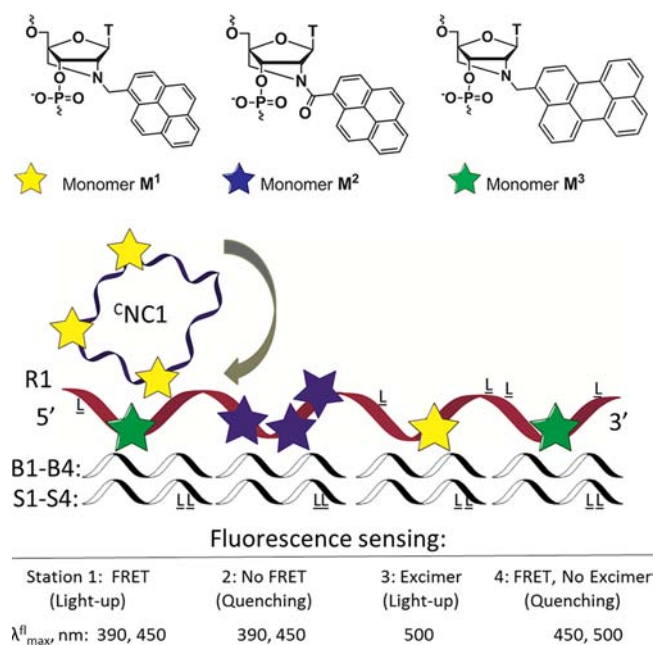


Figure 1. Design of the M^1 – M^3 -labeled nanocrawler, complementary road, and LNA/DNA brake and speed strands (^cNC1, R1, B1–B4, and S1–S4, respectively). The expected fluorescence outputs along the road are also indicated. $\underline{\underline{L}}$ labels denote LNA monomers.

Received: November 15, 2012

Published: February 4, 2013

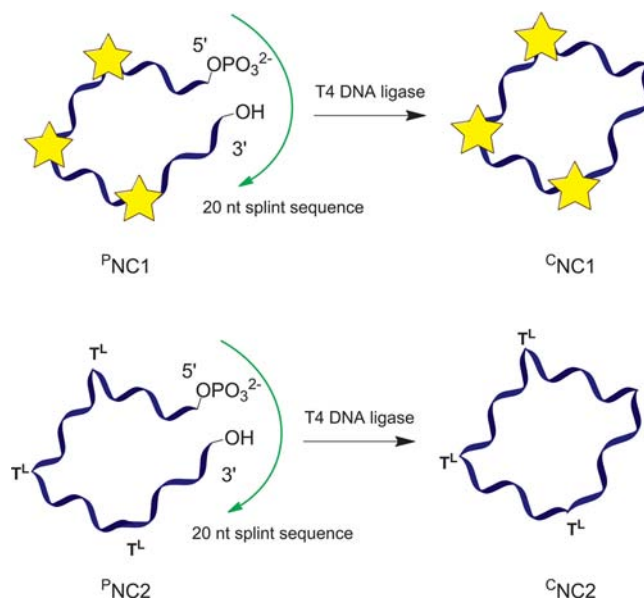
them. For monitoring of the stepwise binding and dissociation between $^{\text{C}}\text{NC1}$ and **R1**, the fluorescence effects of choice were pyrene–perylene FRET of approximately 40% and 100% with $\lambda_{\text{max}}^{\text{fl}} = 450$ nm at stations 1 and 4, respectively, quenching at station 2, and pyrene excimer emission with $\lambda_{\text{max}}^{\text{fl}} = 500$ nm at station 3 (Figure 1). The lengths of the stations and the amounts of additional LNA monomers increased in the 5' → 3' direction of the road, providing lengths of 6, 9, 12, and 15 nt at stations 1–4, respectively [Table S1 in the Supporting Information (SI)]. LNA monomers were incorporated for thermodynamic stability and rigidity of the nanocrawler:road system. The overall length of the road was 42 nt, while the complementary 46 nt nanocrawler contained an additional T nucleotide between each station to ensure rolling of the nanocrawler from the previous station while moving to the next one.

LNA-containing brake strands **B1–B4** were designed as fully complementary sequences to stations 1–4 of the road with 6 nt overhangs at the 5' ends, and the theoretical thermal denaturation temperature (T_{m}) of each brake:road duplex was at least 9 °C higher than that for the corresponding crawler:road complex calculated for each station fragment (Figure S3 and Table S2). Preaddition of the brake strands prevented binding of the nanocrawler to the corresponding region of the road until the corresponding speed strand was added. The speed strands **S1–S4** were fully complementary to **B1–B4**, respectively, with extra LNAs incorporated in the 6 nt overhang region (Table S2). The additional four LNA units in **S1–S4** relative to **B1–B4** resulted in T_{m} values for the brake:speed duplexes that were at least 12 °C higher than those for the corresponding road:brake duplexes, which ensured removal of the brake from the road for effective and also reversible movement of the nanocrawler along the road.

Oligonucleotides containing LNA and monomers M^1 – M^3 were prepared by automated solid-phase phosphoramidite synthesis, purified, and analyzed by matrix-assisted laser desorption ionization mass spectrometry (MALDI MS) and ion-exchange (IE) HPLC according to published procedures (see the SI).⁴ The 46 nt nanocrawler was synthesized as a linear precursor $^{\text{P}}\text{NC1}$ containing a 5'-phosphate group to prepare for concomitant enzymatic cyclization (Scheme 1). The 5'-phosphate group was incorporated using the commercially available CPR II phosphorylation reagent, which was applied during the last step of the automated oligonucleotide synthesis (see the SI). After subsequent dimethoxytrityl (DMT)-on purification, removal of the DMT group, and base-mediated hydrolysis of the 5'-terminal CPR II group, the product $^{\text{P}}\text{NC1}$ was obtained with high purity in sufficient yield (22% after purification starting on a 1 μmol synthesis scale). Additionally, the nonfluorescent LNA/DNA reference sequences $^{\text{P}}\text{NC2}$ and **R2** were synthesized, purified, and further used in the spectral studies described below.

Cyclization of the $^{\text{P}}\text{NC1}$ and $^{\text{P}}\text{NC2}$ strands was performed using T4 DNA ligase and an additional 20 nt splint sequence obtained from a commercial supplier (Scheme 1; also see the SI). Importantly, the starting oligonucleotide concentration was kept low (1 μM), which helped prevent intermolecular polymerization, a side reaction.⁸ The cyclic products were purified by denaturing 13% polyacrylamide gel electrophoresis and characterized by MALDI MS and IE HPLC (see the SI). The overall yields of the cyclized products were 37% ($^{\text{C}}\text{NC1}$) and 42% ($^{\text{C}}\text{NC2}$). Interestingly, a shorter design of the fluorescent nanocrawler containing PAH LNA monomers M^1 located 5 and 4 nt from the 3'- and 5'-termini, respectively, did not yield any cyclic product even at an increased concentration of T4 DNA

Scheme 1. Enzymatic Ligation of the Nanocrawler Linear Precursors Using Splint Sequence and DNA T4 Ligase (Monomer M^1 Is Indicated as a Yellow Star)

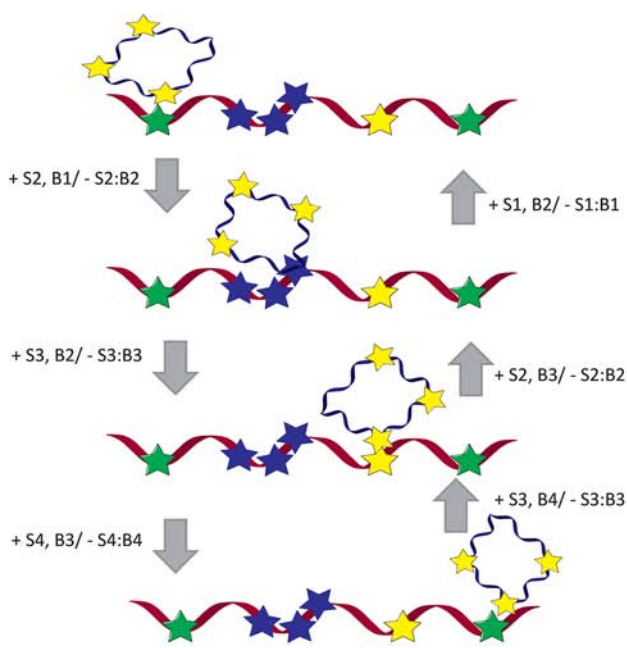


ligase and a longer reaction time (data not shown). We therefore concluded that a longer distance between the terminal reaction sites and the large hydrophobic modification M^1 is essential for efficient recognition of the oligonucleotide substrate by T4 DNA ligase. Interestingly, cyclization of the short nonfluorescent LNA/DNA reference strands was very rapid and successful, underscoring the fact that the smaller LNA modification T^{L} can be recognized much more easily than the M^1 modification by the DNA ligase (data not shown).

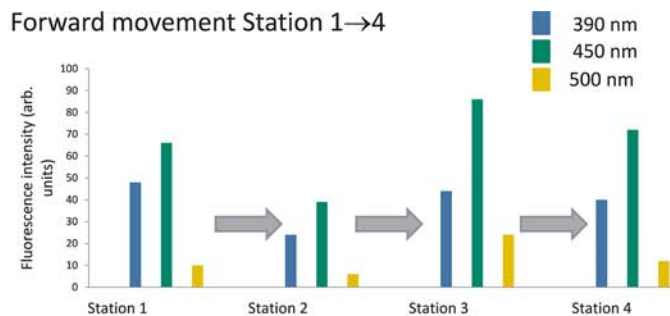
All of the fluorescence experiments were performed in a medium-salt phosphate buffer ($[\text{Na}^+] = 110$ mM) at 19 °C using a single excitation wavelength of 340 nm, and the emission was monitored at $\lambda^{\text{fl}} = 450, 390,$ and 500 nm (Figure 2). The initial spectral studies included measurements of the fluorescence response at each step by adding the nanocrawler to the preannealed road:brake strand complexes, thereby limiting the binding of the nanocrawler exclusively to free regions 1–4 of the road. The resulting reference fluorescence values and representative fluorescence spectra for these reference experiments are reported in the SI.

Next, we performed stepwise reversible movement of the nanocrawler along the road. This was done using the brake and speed strands, and the fluorescence fingerprint signals at every step for monitoring the nanocrawler's position on the road were verified (Figure 2; for the annealing method, see the SI). As can be seen, the nanocrawler interacted with the road:brake strand complexes, giving bright fluorescence responses characteristic of the individual stations and, importantly, consistent with movement in both directions. Since the volume of the sample slightly increased because of the addition of the control strands **B1–B4** and **S1–S4**, the fluorescence analysis was performed using a volume correction, as described in the SI. Using this alignment, we were able to monitor the nanocrawler's movement along the road in both directions without loss of signal for up to 10 cycles (see below and Table S3).

As expected, remarkable fluorescence quenching occurred upon movement of $^{\text{C}}\text{NC1}$ from station 1 to 2, which could be easily seen by the naked eye using a laboratory UV lamp (Figure



Forward movement Station 1→4



Return: Station 4→1

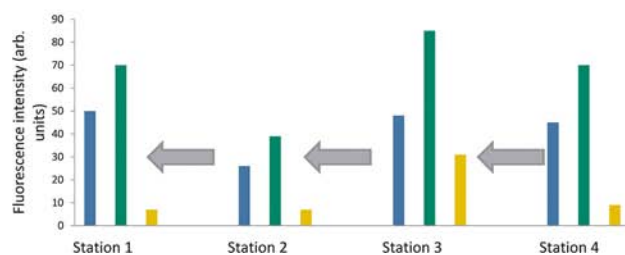


Figure 2. Annealing scheme for the reversible movement of the nanocrawler along the road (left); Fluorescent fingerprint of the movement of the nanocrawler from station 1 to station 4 at 390 nm, 450 and 500 nm (blue, green and yellow bars, respectively) (right).

3). Interestingly, the FRET interaction between monomers M^1 and M^3 was effective already at station 3, as confirmed by a light-



Figure 3. Following the nanocrawler by color changes. Shown left to right are the medium-salt buffer (blank solution) and stations 1–4. The picture was recorded in a medium-salt phosphate buffer using a concentration of $2.0 \mu\text{M}$ for each strand and an excitation wavelength of 365 nm (regular laboratory UV lamp).

up effect at 450 nm and also the excitation spectrum of the system (see the SI). The efficient FRET at station 3 was most likely caused by the close proximity of the multiple pyrene donors and the perylene acceptor already at station 3 (Figure 2). Finally, the excimer signal at $\lambda^{\text{fl}} = 500 \text{ nm}$ was observed exclusively at station 3, giving a specific bright cyan fluorescence at this step. Remarkably, an alternative control strategy using the unbound road and a series of brake strands annealed to the nanocrawler resulted in rapid exchange of the longest brake strand and hybridization of the nanocrawler to the road at station 4 (Figure S3b). Therefore, the road:brake strategy shown in Figures 1 and 2 was optimal for this multistep system, resulting in fully controlled, precise positioning and movements (“crawling”) of the cyclic nanodevice (“nanocrawler”) along the road.

Finally, the binding selectivity of the nanocrawler:road complex during the movement between stations 1 and 4 was investigated (Figure 4). After the preannealed complexes ${}^{\text{C}}\text{NC1:R1:B2-B4}$ and ${}^{\text{C}}\text{NC2:R2:B2-B4}$ were mixed in a 1:1 molar ratio, the two cycles of movement from stations 1 to 4 were performed. Exchange of the fluorescent nanocrawler sequence ${}^{\text{C}}\text{NC1}$ between the fluorescent and nonfluorescent roads R1 and

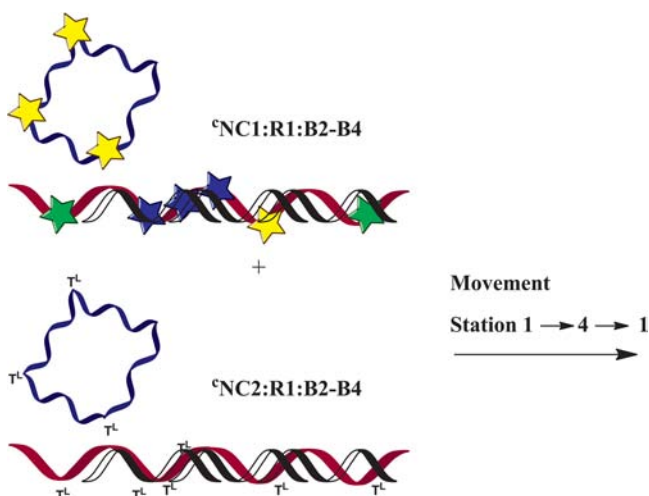


Figure 4. Study of the nanocrawler:road binding selectivity.

R2 would lead to loss of the specific fluorescence signal provided by interstrand interactions between PAH LNAs M^1-M^3 . On the basis of our results, road exchange was not observed at any step of the performed study, confirming the high binding affinity and selectivity of the nanocrawler to its complementary road, which can be attributed to stabilization by multiply inserted affinity-enhancing PAH LNA monomers (Figure S7).⁴ The rolling mechanism was furthermore confirmed by the fact that complete movement of the nanocrawler between nonadjacent stations 1 → 3, leading to a 2.6-fold increase in the fluorescence at 500 nm, was achieved only by reannealing the entire system and not under the conditions for stepwise movement (Figure S8).

In summary, we have built a cyclic LNA/DNA machine that can reversibly move along a complementary road, and its motion can be followed by a specific bright fluorescence response at each station. Current progress in structural DNA nanotechnology and imaging techniques has enabled the preparation and study of more complex DNA nanodevices performing actions in three

dimensions,¹⁰ such as interactions with other biomolecules.¹¹ Supported by rapidly developing DNA modification methods, moieties such as small molecules, polymers,¹² peptides,¹³ and nanoparticles can be attached to such systems.¹⁴ In this context, we believe that the LNA/DNA nanocrawler disclosed herein with its movement-responsive behavior offers appealing opportunities for developing efficient nanomachines as tools for biosensing, pharmacological, and nanoproduction purposes.^{15,16}

■ ASSOCIATED CONTENT

■ Supporting Information

Experimental procedures, including a detailed description of oligonucleotide synthesis, enzymatic ligation, oligonucleotide purification and characterization, and annealing protocols; T_m values and fluorescence intensities; and fluorescence emission and excitation spectra. This material is available free of charge via the Internet at <http://pubs.acs.org>.

■ AUTHOR INFORMATION

Corresponding Author

ias@sdu.dk; jwe@sdu.dk

Notes

The authors declare no competing financial interest.

■ ACKNOWLEDGMENTS

The VILLUM FOUNDATION, The Sapere Aude Programme of The Danish Council for Independent Research, and The Danish National Research Foundation are acknowledged for funding.

■ REFERENCES

- (1) (a) Zhou, C.; Yang, Z.; Liu, D. *J. Am. Chem. Soc.* **2012**, *134*, 1416–1418. (b) Zhang, X.; Yadavalli, V. K. *Nanoscale* **2012**, *4*, 2439–2446.
- (2) Jungmann, R.; Scheible, M.; Simmel, F. C. *Wiley Interdiscip. Rev.: Nanomed. Nanobiotechnol.* **2012**, *4*, 66–81.
- (3) Andersen, E. S.; Dong, M.; Nielsen, M. M.; Jahn, K.; Subramani, R.; Mamdouh, W.; Golas, M. M.; Sander, B.; Stark, H.; Oliveira, C. L. P.; Pedersen, J. S.; Birkedal, V.; Besenbacher, F.; Gothelf, K. V.; Kjems, J. *Nature* **2009**, *459*, 73–77.
- (4) For the use of PAH LNA in nucleic acid nanotechnology, see: (a) Wengel, J. *Org. Biomol. Chem.* **2004**, *2*, 277–280. (b) Kalra, N.; Babu, B. R.; Parmar, V. S.; Wengel, J. *Org. Biomol. Chem.* **2004**, *2*, 2885–2887. (c) Hrdlicka, P. J.; Babu, B. R.; Sørensen, M. D.; Wengel, J. *Chem. Commun.* **2004**, 1478–1479. (d) Gupta, P.; Langkjær, N.; Wengel, J. *Bioconjugate Chem.* **2010**, *21*, 513–520 and articles cited therein. (e) Astakhova, I. V.; Lindegaard, D.; Malakhov, A. D.; Korshun, V. A.; Wengel, J. *Chem. Commun.* **2010**, 46, 8362–8364.
- (5) For some recent examples of various modified nucleotide analogues in nucleic acid nanotechnology, see: (a) Cherkasov, D.; Biet, T.; Bäuml, E.; Traut, W.; Lohoff, M. *Bioconjugate Chem.* **2010**, *21*, 122–129. (b) Kricka, L. J.; Fortina, P. *Clin. Chem.* **2009**, *55*, 670–683 and articles cited therein.
- (6) Genot, A. J.; Bath, J.; Turberfield, A. J. *J. Am. Chem. Soc.* **2011**, *133*, 20080–20083.
- (7) El-Sagheer, A. H.; Brown, T. *Acc. Chem. Res.* **2012**, *45*, 1258–1267.
- (8) Diegelman, A. M.; Kool, E. T. *Curr. Protoc. Nucleic Acid Chem.* **2000**, 5.2.1–5.2.27.
- (9) For example, see: Pinheiro, V. B.; Taylor, A. I.; Cozens, C.; Abramov, M.; Renders, M.; Zhang, S.; Chaput, J. C.; Wengel, J.; Peak-Chew, S.-Y.; McLaughlin, S. H.; Herdewijn, P.; Holliger, P. *Science* **2012**, *336*, 341–344.
- (10) Omabegho, T.; Sha, R.; Seeman, N. C. *Science* **2009**, *324*, 66–71.
- (11) Selmi, D. N.; Adamson, R. J.; Attrill, H.; Goddard, A. D.; Gilbert, R. J. C.; Watts, A.; Turberfield, A. J. *Nano Lett.* **2011**, *11*, 657–660.
- (12) Sun, Y.; Liu, H.; Xu, L.; Wang, L.; Fan, Q.-H.; Liu, D. *Langmuir* **2010**, *26*, 12496–12499.
- (13) Williams, B. A. R.; Diehnelt, C. W.; Belcher, P.; Greving, M.; Woodbury, N. W.; Johnston, S. A.; Chaput, J. C. *J. Am. Chem. Soc.* **2009**, *131*, 17233–17241.
- (14) Lo, P. K.; Karam, P.; Aldaye, F. A.; McLaughlin, C. K.; Hamblin, G. D.; Cosa, G.; Sleiman, H. F. *Nat. Chem.* **2010**, *2*, 319–328.
- (15) Li, D.; Song, S.; Fan, C. *Acc. Chem. Res.* **2010**, *43*, 631–641.
- (16) Mershin, A.; Cook, B.; Kaiser, L.; Zhang, S. *Nat. Biotechnol.* **2005**, *23*, 1379–1380.